

THE DEPENDENCE OF SUBHALO ABUNDANCE ON HALO CONCENTRATION

YAO-YUAN MAO¹, MARC WILLIAMSON, AND RISA H. WECHSLER²

Kavli Institute for Particle Astrophysics and Cosmology & Physics Department, Stanford University, Stanford, CA 94305, USA and
SLAC National Accelerator Laboratory, Menlo Park, CA, 94025, USA

Draft version August 11, 2015

ABSTRACT

Hierarchical structure formation implies that the number of subhalos within a dark matter halo depends not only on halo mass, but also on the formation history of the halo. This dependence on the formation history, which is highly correlated with halo concentration, can account for the super-Poissonian scatter in subhalo occupation at a fixed halo mass that has been previously measured in simulations. Here we propose a model to predict the subhalo abundance function for individual host halos, that incorporates both halo mass and concentration. We combine results of cosmological simulations with a new suite of zoom-in simulations of Milky Way-mass halos to calibrate our model. We show the model can successfully reproduce the mean and the scatter of subhalo occupation in these simulations. The implications of this correlation between subhalo abundance and halo concentration are further investigated. We also discuss cases in which inferences about halo properties can be affected if this correlation between subhalo abundance and halo concentration is ignored; in these cases our model would give a more accurate inference. We propose that with future deep surveys, satellite occupation in the low-mass regime can be used to verify the existence of halo assembly bias.

Keywords: dark matter — galaxies: halos — methods: analytical — methods: numerical

1. INTRODUCTION

Bridging our understanding of the processes of galaxy formation and of the evolution of dark matter halos remains one of the primary challenges in modern cosmology. While N -body simulations provide detail about the formation and evolution of dark matter halos, it is still observationally challenging to directly probe their properties. Nevertheless, extensive work over the past decade has used observations of galaxy's spatial distributions to constrain models of the galaxy-halo connection, which reveals how galaxies form in halos (e.g., [Berlind & Weinberg 2002](#); [Zehavi et al. 2011](#); [Reddick et al. 2013](#)). As new observations become more precise, it is crucial to understand possible systematic uncertainty and bias in those models.

The two main characteristics of a dark matter halo are its mass, usually calculated by setting a spherical overdensity region, and its formation history. The latter is also highly correlated with the density profile of the halo, and hence with the concentration and with the maximal circular velocity v_{\max} of the halo ([Wechsler et al. 2002](#)). Halos of the same mass but different formation history can have very different characteristics or reside in different environments (e.g., [Bullock et al. 2001](#); [Allgood et al. 2006](#); [Macciò et al. 2007](#)).

The abundance of subhalos within a dark matter halo most strongly correlates with the mass of the halo (e.g., [Kravtsov et al. 2004](#)). Nevertheless, at a fixed halo mass, the subhalo abundance also correlates with the formation history of the halo ([Zentner et al. 2005](#); [Zhu et al. 2006](#); [Ishiyama et al. 2009](#)). This correlation, despite its significance in modeling satellite occupation, is often neglected, mostly because it does not manifest itself when the Poisson scatter is comparable to the number of subhalos in

consideration. Satellite occupation, or richness, is often used as a proxy of host halo mass, especially for optical observations of clusters ([Roza et al. 2009, 2010](#)). The scatter in the mass distribution inferred from richness can be underestimated if this correlation with concentration is neglected.

In this work, we investigate again the correlation between subhalo abundance and halo concentration, and propose a simple model that describes this correlation. This model can also be used to extend the subhalo abundance function for a given host halo beyond the resolution limit, and enables us to evaluate how this correlation may manifest in a range of observable statistics.

The simplest approach to extend the subhalo abundance function beyond the resolution limit is to extrapolate a parametrized subhalo abundance function. The subhalo abundance function is most commonly modeled by a power law, and the parameters of the model can be calibrated against simulations. Studies have shown this method describes the subhalo abundance functions in N -body simulations very well ([Gao et al. 2004](#); [Kravtsov et al. 2004](#); [Giocoli et al. 2008](#); [Springel et al. 2008](#); [Angulo et al. 2009](#); [Boylan-Kolchin et al. 2010](#); [Ishiyama et al. 2013](#); [Cautun et al. 2014b](#)), at least for host halos in a narrow mass range.

In order to calibrate this kind of model over a wide range of mass, usually a suite of cosmological simulations and zoom-in simulations is needed. Zoom-in simulations, such as the Aquarius and Phoenix simulations ([Springel et al. 2008](#); [Gao et al. 2012](#)), are particularly powerful for measuring subhalo abundance function at high resolution but still with reasonable costs. However, if one wants to study the halo-to-halo scatter in the subhalo abundance function, a fairly large sample size is required. More recently, two re-simulation suites have been completed with tens to hundreds of simulations in specific small mass ranges: the Rhapsody (cluster-mass halos, [Wu et al.](#)

¹ yymao@stanford.edu

² rwechsler@stanford.edu

2013) and ELVIS simulations (Milky Way-mass halos, Garrison-Kimmel et al. 2014).

While these fitting models can usually describe simulations fairly well, they often capture the minimal relevant physics for the particular questions that are being addressed. A more elaborate approach is to consider the assembly histories of dark matter halos and the evolution of halo mass function (Yang et al. 2011). One can further consider more relevant subhalo dynamics when modeling subhalo abundance beyond the resolution limit by tracking the orbits of subhalos and adding subhalos that do not appear or are disrupted in simulations (Zentner et al. 2005; Jiang & van den Bosch 2014; van den Bosch & Jiang 2014). Instead of fitting the abundance function, this kind of approach considers most physical details, but at the same time can be more difficult to constrain.

In this work, we focus on an empirical model which directly uses mass and v_{\max} of the host halo to predict the subhalo abundance function, and calibrate the model against cosmological and zoom-in simulations. This model is essentially the simplest possible model of subhalo abundance function that takes halo formation history into account. In principle, a more sophisticated model (i.e., models that track subhalo evolution) could produce similar results. However, our simple model provides a straightforward way to evaluate this correlation between subhalo abundance and halo formation history, and to evaluate its implications for various observables.

This paper is organized as follows. In Section 2 we describe the simulations used in this study. In Section 3 we first discuss the correlation between subhalo abundance and halo formation history, and then we describe and calibrate the model which predicts the subhalo abundance. In Section 4, we further discuss the implications of this correlation between subhalo abundance and halo concentration. We summarize this paper in Section 5.

2. SIMULATIONS

In this study we use a cosmological simulation c125-2048 and also present a new set of zoom-in simulations of Milky Way-mass halos.

The c125-2048 box³ is a dark matter-only cosmological simulation run with L-GADGET (based on GADGET-2, Springel et al. 2001; Springel 2005). The box has 2048^3 particles and a side length of $125 \text{ Mpc } h^{-1}$, resulting in a particle mass of $1.8 \times 10^7 M_{\odot} h^{-1}$. The softening length used is $0.5 \text{ kpc } h^{-1}$, constant in comoving length. The cosmological parameters are $\Omega_m = 0.286$, $\Omega_{\Lambda} = 0.714$, $h = 0.7$, $\sigma_8 = 0.82$, and $n_s = 0.96$. The initial conditions are generated by 2LPTIC⁴ (Crocce et al. 2006) at $z = 199$, with the power spectrum generated by CAMB.⁵

The new suite of zoom-in simulations consists of 46 Milky Way-mass halos, selected from the c125-1024 box (see footnote 3), which is a low-resolution version of the c125-2048 box. The parameters and initial conditions of these two boxes are identical, but c125-1024 contains only 1024^3 particles and starts at $z = 99$. All the selected halos fall in the mass range $M_{\text{vir}} = 10^{12.1 \pm 0.03} M_{\odot}$ in the

c125-1024 box. The initial conditions of these zoom-in simulations are generated with the publicly available MUSIC code⁶ (Hahn & Abel 2011), and are matched to the cosmological box up to the 1024^3 scale. The Lagrangian volume where the highest-resolution particles are placed is set by the rectangular volume which the particles within $10R_{\text{vir}}$ of the present-day halo occupied at $z = 99$. The mass of the highest-resolution particles in the zoom-in simulations is $3.0 \times 10^5 M_{\odot} h^{-1}$. The softening length in the highest-resolution region is $170 \text{ pc } h^{-1}$ comoving. Figure 1 shows the images of 6 of these zoom-in simulations. Figure 2 compares the concentration distribution of this sample of Milky Way-like halos with the full sample in the mass range in the c125-2048 box. The concentration distribution of the selected sample is slightly wider than that of all the host halos in the mass range.

In the analysis, we use ROCKSTAR⁷ for halo finding and CONSISTENT TREES⁸ for tree building (Behroozi et al. 2013a,b). The halos are defined with $\Delta_{\text{vir}} \simeq 99.2$ for this cosmology. Subhalos are defined as halos that are within R_{vir} of any other larger halo. Halos that are not a subhalo are called *host halos* throughout this paper.

The particle mass of a simulation cannot be directly translated into the maximal circular velocity, v_{\max} , to which the simulation converges. By inspecting the velocity function, we estimate that a conservative lower limit for the convergence of the c125-2048 box is 40 km s^{-1} , and that of the zoom-in Milky Way simulations is 9 km s^{-1} .

3. MODELING SUBHALO ABUNDANCE

In this section, we present a framework to model the subhalo abundance of individual host halos. We first discuss the correlation between subhalo abundance and host halo concentration, and observe qualitatively how host halo concentration affects subhalo abundance function. We further argue that for a given host halo, the number of subhalos is consistent with a Poisson distribution. Then we describe both the framework and the specific parameterization of our model, and calibrate the model against the aforementioned simulations. Finally we briefly discuss the universality of the subhalo abundance function.

3.1. Dependence of Subhalo Abundance on Halo Concentration

N -body simulations have shown that the subhalo abundance function averaged over a sample of host halos of a similar mass approximately follows a power law, and its form is nearly universal for different host halo masses when scaled properly (e.g., Gao et al. 2004; Kravtsov et al. 2004; Boylan-Kolchin et al. 2010). Hence, the simplest model of subhalo abundance is to describe the mean number of subhalos, $\langle N_{\text{sub}} \rangle$, as a function of host halo mass only. Although this simple kind of model can predict the mean number of subhalos at a given host halo mass in simulations fairly well, it cannot explain the dependence of subhalo abundance on host halo concentration, as shown in Zentner et al. (2005).

³ Provided by Matthew Becker (M. Becker et al. 2015, in preparation)

⁴ <http://cosmo.nyu.edu/roman/2LPT/>

⁵ <http://camb.info/>

⁶ <https://bitbucket.org/ohahn/music>

⁷ <https://bitbucket.org/gfcstanford/rockstar>

⁸ <https://bitbucket.org/pbeherozi/consistent-trees>

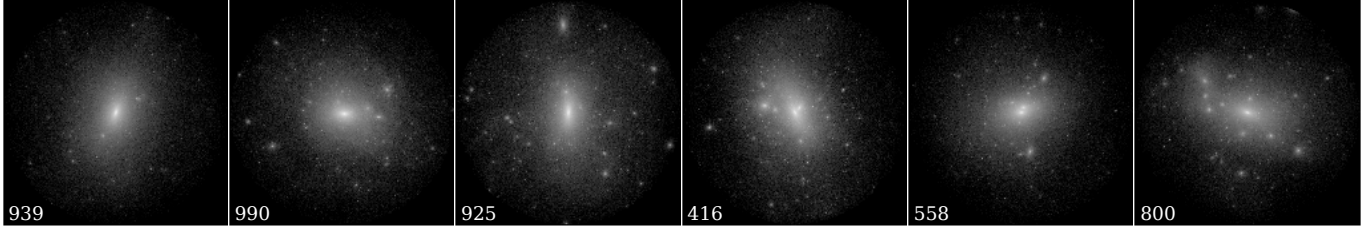


Figure 1. Images of the zoom-in simulations of six Milky Way-mass halos, from our suite of 46 halos. The concentration of these selected halos decreases from left to right.

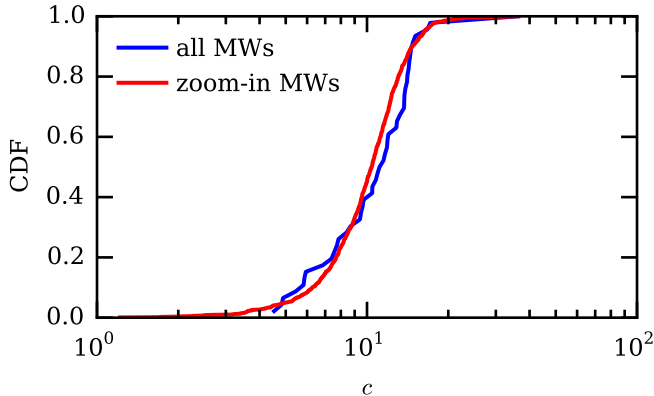


Figure 2. The cumulative distribution of concentration (in log scale) for the zoom-in Milky Way halos (red) and all the halos in the same mass range in thec125-1024 box (blue).

To see how host halo concentration affects the number of subhalos, in [Figure 3](#) we plot the mean number of halos (including hosts and subhalos) whose v_{\max} (or v_{peak}) is larger than 60 km s^{-1} (or 75 km s^{-1}) as a function of host halo mass. We plot this relation for all the host halos and for only halos with the highest and the lowest 25% of concentration in each mass bin. We can clearly see that halos of high concentration tend to have fewer subhalos, and also see that this is not a small effect, especially when the host halo mass is about $10^{12} M_{\odot} h^{-1}$. We note that at higher host halo mass, this difference becomes smaller because high-mass halos have a smaller spread in concentrations than low-mass halos.

We now take a closer look at how concentration affects the subhalo abundance on a halo-by-halo basis for host halos of the same mass. In [Figure 4](#), we plot the subhalo v_{\max} function for all the zoom-in simulated Milky Way-mass halos. The subhalo v_{\max} functions in [Figure 4](#) are colored according to the concentration of their respective host halos. We observe two prominent features:

1. All these halos fall in a very narrow mass bin (smaller than 0.08 dex), yet there is a significant halo-to-halo scatter in their subhalo v_{\max} functions. The halo-to-halo scatter seems to affect mostly the normalization of the subhalo v_{\max} function, and the trend roughly follows the concentration trend, which is indicated in colors — darker lines sit lower.
2. On the log-log plot, subhalo v_{\max} functions are mostly parallel to one another, especially in the regime where $N_{\text{sub}} > 10$. This suggests the power-law index is roughly a constant from halo to halo. Also, for each individual halo, the deviation of the abundance function from a simple power law is

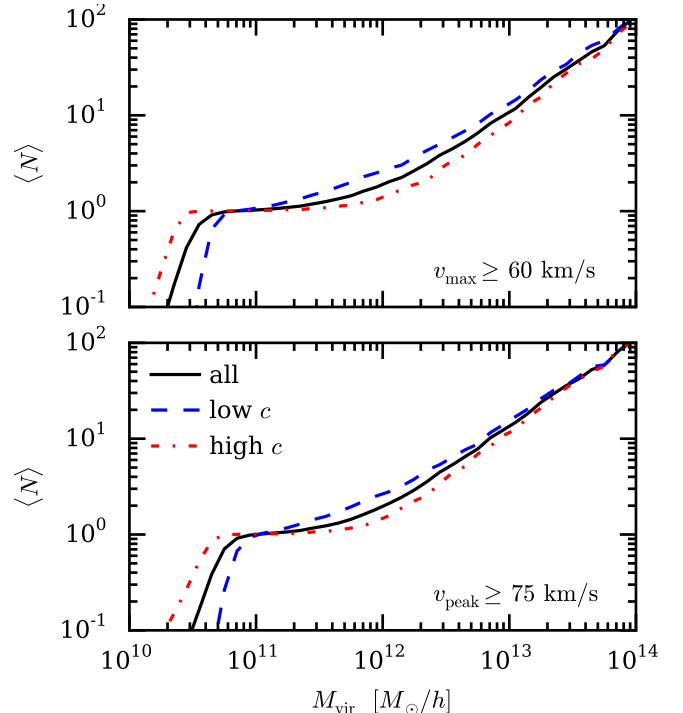


Figure 3. Number of *galaxies*, i.e., halos (including both hosts and subhalos) with a cut in v_{\max} (upper) or in v_{peak} (lower), as a function of host halo mass. The black solid line shows all host halos, while the blue dashed line and the red dash-dot line show the host halos with the lowest and the highest 25% of concentration, respectively.

much smaller than the halo-to-halo scatter when N_{sub} is large.

In [Wu et al. \(2013\)](#), the authors also find that the numbers of subhalos in different v_{\max} bins are correlated, especially when N_{sub} is large. This agrees with our findings here.

This correlation between the subhalo number and host halo concentration has been found and discussed in, for example, [Zentner et al. \(2005\)](#), [Watson et al. \(2011\)](#). This correlation can be understood by the hierarchical formation of halos: conditioned on a fixed halo mass, halos with higher concentration form early, and subhalos in these halos are stripped longer to a lower mass and v_{\max} , and some could already be completely disrupted and merged with the host. Both effects would result in a smaller number of subhalos at a fixed velocity cut.

3.2. Small-scale Poisson Scatter

It is also known and shown explicitly by [Boylan-Kolchin et al. \(2010\)](#) that the scatter in the number

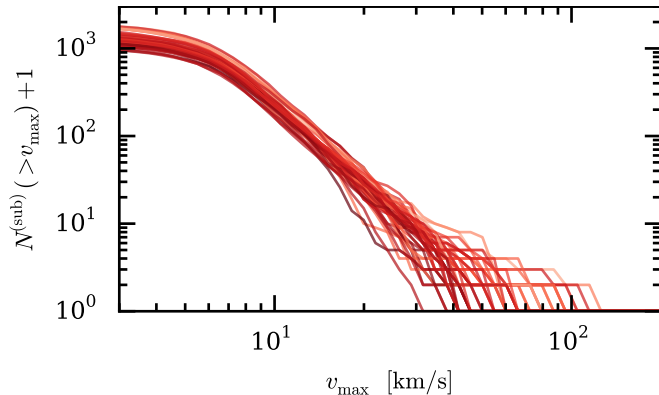


Figure 4. The subhalo v_{\max} function for the 46 zoom-in simulations of the Milky Way halos. Each line represents one host halo and is colored according to the ratio V_{\max}/V_{vir} of the host halo. Darker color represents halos of higher concentration (larger V_{\max}/V_{vir}). The gray band on the left shows the regime affected by resolution, where the abundance function bends due to unresolved subhalos.

of subhalos is super-Poissonian when the mean number is much larger than 1, The authors argue this super-Poissonian scatter is a sum of a Poisson scatter and an *intrinsic* scatter (see also related discussion in Busha et al. 2011b).

Here we further claim that the Poisson scatter should exist on a single-halo basis. That is, given a host halo and its environment, the small-scale variation would result in a Poisson scatter in its subhalo abundance. On the other hand, the *intrinsic* scatter (or more precisely called the *halo-to-halo* scatter) is then in principle all possible scatter among host halos.

To verify that the subhalo abundance function is always subject to this small-scale Poisson scatter when we consider a single host halo, i.e.,

$$(N_{\text{sub}}|\text{host}) \sim \text{Pois}(\langle N_{\text{sub}}|\text{host} \rangle), \quad (1)$$

we run 13 zoom-in simulations of a single halo, with different random seeds for the small-scale modes. All these 13 realizations have the same simulation setup as described above, and also the same large-scale initial conditions down to the scale of $k \sim 16.4 h \text{ Mpc}^{-1}$, which is equivalent to 2048^3 particles in the box. This scale roughly corresponds to a host halo mass of $2.5 \times 10^{10} M_{\odot} h^{-1}$, or host $V_{\max} \sim 50 \text{ km s}^{-1}$.

Figure 5 shows $\sigma/\sigma_{\text{Pois}}$, where σ is standard deviation and $\sigma_{\text{Pois}} = \sqrt{\langle N \rangle}$, i.e., the square-rooted ratio of the variance to the mean of the number of subhalos, in bins of v_{\max} of the subhalos. The variance and the mean are calculated over the 13 halos of the same large-scale initial conditions. If the number of subhalos in a given v_{\max} bin follows a Poisson distribution, this ratio would be 1. In Figure 5, one can see that at higher values of v_{\max} , this ratio is less than 1, which is expected due to the constrained large-scale modes. At smaller v_{\max} , this ratio approaches 1. Although the sample size is small, the typical number of subhalos above $v_{\max} = 10 \text{ km s}^{-1}$ is already more than 200. Hence, if the super-Poissonian scatter truly exists at the scales within a single host halo, one would expect the ratio to be larger than 1 at small v_{\max} , scaling similar to the green dashed line, which includes the super-Poissonian scatter. This test suggests that, for a *given* host halo (and its environment), the

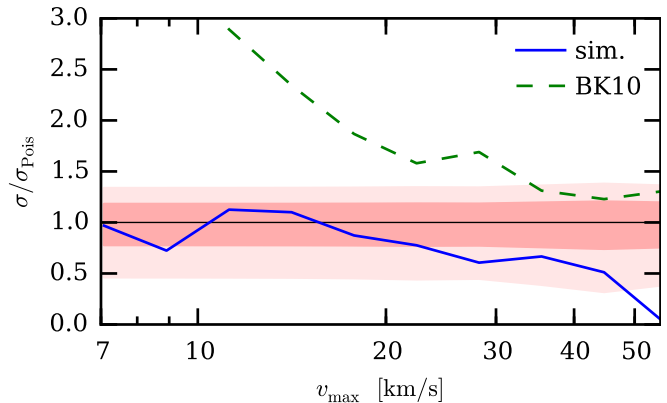


Figure 5. The blue line shows $\sigma/\sigma_{\text{Pois}}$ in bins of v_{\max} , calculated over the 13 halos of the same large-scale initial conditions. The red bands show the 1- σ (dark) and 2- σ (light) confidence interval if N follows a Poisson distribution and given that there are 13 samples. The green dashed line shows the super-Poissonian scatter (Boylan-Kolchin et al. 2010, Figure 8) for comparison.

scatter of its subhalo abundance is consistent with Poisson scatter. The super-Poissonian scatter in a fixed host halo mass cannot solely come from small-scale modes, and should be a result of the scatter in the host halo properties at that fixed mass, combined with dependence of the subhalo abundance on these properties.

3.3. Framework of the Model

Now we present the framework of our subhalo abundance model. We first outline our model that describes the number of subhalo for a given host halo, and the parameters of the model. Then we further present how to relate these model parameters to the properties of the host halos. In this fashion, we can clearly separate the Poisson scatter in each individual host halo from the halo-to-halo scatter.

Mathematically, we can model the subhalo abundance function as a counting process. Here the counting process we consider is counting over the proxy variable (i.e., v_{\max} or M_{vir}), not over the physical time. Although the mathematical term we used is *process*, we are not considering the physical evolution of the subhalo merging process, but only the number of subhalos at a given time.

Let $N(v)$ denote the number of subhalos whose v_{\max} (or other proxy, which for simplicity we call v) is greater than or equal to v . Note that $N(v)$ is always an integer and has the following properties:

$$N(v_1) \geq N(v_2), \text{ if } v_1 \leq v_2, \quad (2a)$$

$$N(v) = 0, \text{ if } v \geq V_{\text{cut}}, \quad (2b)$$

where V_{cut} is a scale above which there are no subhalos. The value of V_{cut} depends on the host halo.

We further argue that this counting process is an inhomogeneous Poisson process. That is, the number of subhalos in the interval $[v_1, v_2]$ follows a Poisson distribution and is independent of the counts in any other disjoint intervals. We can write

$$[N(v_1) - N(v_2)] \sim \text{Pois}(\lambda(v_1, v_2)), \quad (3)$$

and

$$\lambda(v_1, v_2) = \left(\frac{v_1}{V_0}\right)^n - \left(\frac{\min(v_2, V_{\text{cut}})}{V_0}\right)^n, \quad (4)$$

where V_0 is a positive parameter and n is a negative parameter, and both could depend on the host halo. Note that the parameters V_0 and V_{cut} should have the unit of the proxy. For example if the proxy is v_{max} , they should have the unit of velocity. If one uses M_{vir} instead as the proxy, they should have the unit of mass.

The expected number of subhalos whose $v_{\text{max}} \geq v$ is then simply

$$\langle N(v) \rangle = \left(\frac{v}{V_0} \right)^n - \left(\frac{V_{\text{cut}}}{V_0} \right)^n. \quad (5)$$

We note that by introducing the V_{cut} scale, we do not need an additional exponential cutoff in the model. The average subhalo abundance function naturally drops off at the high end, and resembles an exponential cutoff. There are two strengths of this approach. First, the parameter V_{cut} has a clear physical meaning; no subhalo can have v_{max} (or any proxy in use) that is larger than V_{cut} . Second, when implementing this model, one does not need to worry about the chance of having a subhalo with a very large v_{max} . The chance of having such an outlier is remote but still finite when using an exponential cutoff, while in our model the probability of a subhalo with $v_{\text{max}} \geq V_{\text{cut}}$ is zero by construction.

With our framework, there is a straightforward algorithm to create a set of values which represents the set of the subhalo v_{max} values of a particular host halo, given a known threshold v_{thres} . This algorithm helps to generate a mock catalog of subhalos beyond the resolution limit. To generate this set, one first draws one random number k from a Poisson distribution of mean $N(v_{\text{thres}})$ according to Equation (5), with v_{thres} being the minimal possible v_{max} value in the desired set. Then one draws k random numbers X_1, \dots, X_k from a uniform distribution $\mathcal{U}(0, 1)$. The desired set would then be $\{f(X_1), \dots, f(X_k)\}$, where

$$f(x) := V_0 \left[N(v_{\text{thres}}) \cdot x + \left(\frac{V_{\text{cut}}}{V_0} \right)^n \right]^{1/n} \quad (6)$$

is the inverse function of Equation (5).

3.4. Calibrating the Model

So far we have introduced three parameters that are associated with the host halo: V_{cut} , the largest scale a subhalo could have; V_0 , the overall normalization of the subhalo abundance function; and n , the power-law index (log-log slope) of the subhalo abundance function. In principle, the values of these three parameters in different host halos do not need to follow any universal relation, and can depend on *any* host halo property. Nevertheless, since the dark matter halos in dissipationless simulations do have many universal properties, it is plausible that some universal relations relating these three parameters to the host halo properties would already make a good approximation.

For conventional models that describe $\langle N \rangle$ as a function of host halo mass only, one can parameterize the variables in Equation (4) as follows

$$V_0 = a V_{\text{vir}}, \quad (7a)$$

$$V_{\text{cut}} = b V_{\text{vir}}, \quad (7b)$$

$$n = n_0, \quad (7c)$$

Table 1
Parameter Values

Proxy	Redshift	a_0	α	b_0	β	n_0
v_{max}	0	0.49	-0.9	1.4	-2.5	-2.90
v_{max}	1	0.85	-1.0	1.4	-1.0	-2.80
v_{max}	3	1.70	-1.0	1.4	-0.8	-2.60
v_{peak}	0	0.67	-0.8	1.4	-2.5	-2.75

Note. — See Equations (7) and (8) for the definitions of these parameters. See text of Section 3.4 for details.

where V_{vir} refer to the circular velocity at R_{vir} of the host halo, a , b , and n_0 are all constants that do *not* depend on any host halo properties.

However, we already know that the parameterization above cannot account for the dependence on halo concentration. Here we present a specific parameterization that replaces a and b in Equations (7) with functions of $(V_{\text{max}}/V_{\text{vir}})$. Particularly, we set

$$a := a_0 \left(\frac{V_{\text{max}}}{V_{\text{vir}}} \right)^\alpha, \quad (8a)$$

$$b := b_0 \left(\frac{V_{\text{max}}}{V_{\text{vir}}} \right)^\beta, \quad (8b)$$

where a_0 , b_0 , α , and β are constant. Here V_{vir} and V_{max} refer to the host halo, and their ratio can be viewed as a proxy of the halo concentration or formation time. When $\alpha = \beta = 0$, this falls back to the conventional model which has no concentration dependence.

With this particular parametrization which incorporates host halo concentration, we can calibrate the model against simulations. With the c125-2048 box, we find the values listed in Table 1 provide decent descriptions to both the mean and the scatter of subhalo abundance across a wide range of mass. We also find the values for two different redshifts ($z = 1$ and 3) and for using v_{peak} as the proxy. Note that if one use v_{peak} as the proxy instead of v_{max} , the dependence on concentration is slightly weaker (see the values of α in Table 1).

Figure 6 compares simulations with the prediction from this model with the parameters listed in Table 1. In the simulations, we bin host halos according to their mass, in a wide range of masses (10^{12} – $10^{14} M_\odot h^{-1}$), and measure the mean and variance of number of subhalos whose $v_{\text{max}} > 50 \text{ km s}^{-1}$ in each bin. For each host halo we also predict the number of subhalos with the model, and measure the binned mean and variance in the same way as with simulations. Then we plot the relative difference between the model prediction and the simulation as a function of host halo mass in Figure 6. The relative difference is defined as $\delta X := X_{\text{model}}/X_{\text{sim}} - 1$, where X could be the mean (upper panels) or variance (lower panels) of number of subhalos in each mass bin.

As Figure 6 shows, our model can reproduce the mean and variance of the number of subhalos in all mass bins very well. We also plot the model with *no* concentration dependence ($\alpha = \beta = 0$) for comparison. While this kind of model can reproduce the mean value, it fails to reproduce the variance. Especially for the predicted variance, our model successfully recovers the scatter in high-mass bins, where a model that depends only on mass or the Poisson scatter cannot. For halos of the highest and the

lowest 25% concentration in each mass bin, our model also fits the simulation reasonably well.

In this work, we do not focus on refining these relations to obtain the best mock subhalo abundance function. In fact, the essence of this work is to show that with our simple model one can already reproduce most important features in the subhalo abundance function. There are two main reasons for not pursuing the *best-fit* model here.

First of all, the parameterization proposed above is not unique. For example, one can substitute the ratio V_{\max}/V_{vir} that appears in V_0 with some generic function of concentration $f(c)$, or put in a mass/velocity dependency in n . The parameters can also involve other host properties, or even be stochastic (i.e., involving random variables). Also, while the parameters provide insight on the dependence on concentration, they do not bear clear physical meaning and the parameterization choice is somewhat arbitrary.

Second, although simulations do provide constraints on the model parameters, these parameters are very degenerate and the Poisson scatter of individual halos makes it very difficult to tightly constrain the *best-fit* parameters. Multiple sets of values could give equally good fits to simulations, and the choice of the objective function (statistics to minimize) would also affect the best-fit values. The reported value in [Table 1](#) are obtained by fitting only the mean and scatter of subhalo abundance in the full c128–2048 box in bins of host halo mass (i.e. to minimize the two leftmost panels in [Figure 6](#)), yet these values also provide decent fits to the individual abundance function as shown in [Figure 7](#).

As a result, here we do not give meaningful error bars on the parameter values, but rather simply demonstrate the model’s capability of reproducing the subhalo abundance functions. Until the statistics of high-resolution halos improves significantly, we recommend optimizing the fit every time for each specific use case.

3.5. The Power-law Index

So far we have been fixing the power-law index (log–log slope) to be a constant that does not change with halo properties when calibrating our model against the c125–2048 box. This assumption is consistent with previous studies (e.g., [Gao et al. 2012](#)). However, due to the resolution limit, low-mass host halos in a cosmological box do not constrain the index as well as the high-mass halos because the number of resolved subhalos in low-mass host halos is smaller and subject to larger relative Poisson scatter. As a result, the value of n_0 in [Table 1](#) is mostly set by those high-mass halos in the box.

To investigate whether the power-law index is indeed a constant, we check if the model would work for both the zoom-in Milky Way halos and the high-mass halos in the box. In [Figure 7](#) we compare the subhalo abundance function in simulations with that predicted by the model. We discover that a constant index which can fit the subhalo abundance function very well for cluster-size halos fails to fit the abundance function for zoom-in Milky Way-size halos. The log–log slope of the abundance function is steeper for Milky Way-size halos than for cluster-size halos.

We emphasize again that this mass trend is difficult to detect in a cosmological box due to limited dynamical range. As shown in the upper right panel of [Figure 7](#),

at $v_{\max} = 50 \text{ km s}^{-1}$, both the number of subhalos and the scatter are still consistent with the prediction from a constant slope.

Recall that the power-law index also changes with redshift, as shown in [Table 1](#): at higher redshift, the log–log slope of the abundance function is shallower. The relation between the power-law index, host halo mass, and redshift is also discussed in [Zentner et al. \(2005\)](#), [Watson et al. \(2011\)](#). An intriguing question is then whether this redshift trend and the aforementioned mass trend in the index have the same physical origin.

Specifically, we find that we can fit the subhalo v_{\max} functions of the zoom-in Milky Way halos and of the cosmological box simultaneously (see the lower panels of [Figure 7](#)) if we replace the constant index by this relation,

$$n = -3.05 \nu(M, z)^{-0.1}, \quad (9)$$

where

$$\nu(M, z) = \frac{\delta_c}{\sigma(M)D(z)},$$

$\delta_c \approx 1.686$ is the critical overdensity, $D(z)$ is the linear growth rate, and $\sigma(M)$ is the squared root of the mass variance (at $z = 0$) with a top-hat filter of mass M .

[Figure 8](#) shows the relation of Equation (9) and compares it with the constant values of n_0 in [Table 1](#). Although this is *not* a proof of the validity of Equation (9), it indeed demonstrates the possibility that the mass and redshift trends in the power-law index have the same physical origin. To robustly verify this connection between n and $\nu(M, z)$ would require several sets of zoom-in simulations of halos of different masses, preferably also with different cosmologies. This is beyond the scope of this work, but worth exploring as simulation suites expand.

4. IMPLICATIONS AND DISCUSSION

So far we have been focusing on *subhalo* abundance function and its dependence on host halo concentration. In this section, we discuss its observational implications. While we cannot observe dark matter subhalos directly, we can certainly count the satellite galaxies that sit in those subhalos. Hence, the *subhalo* occupation can be viewed as a proxy of the *satellite* occupation, subject to the effect of baryons on the subhalo abundance function (e.g., [Cui et al. 2012](#); [Vogelsberger et al. 2014](#)). Here we ignore baryonic effects and directly translate the subhalo occupation above a certain velocity cut to the satellite abundance at a luminosity threshold by specifying a galaxy–subhalo connection.

The simplest relation between subhalos and satellite galaxies is a one-to-one relation,

$$N_{\text{sub}}(> v) = N_{\text{sat}}(> L(v)), \quad (10)$$

where $L(v)$ specifies the correspondence between velocity cut and luminosity threshold by matching their abundance functions. This is commonly known as *abundance matching* (e.g., [Kravtsov et al. 2004](#); [Vale & Ostriker 2004](#)), which has been shown to work fairly well for predicting measurements such as the correlation functions (e.g., [Conroy et al. 2006](#); [Reddick et al. 2013](#)). With this abundance matching scheme, the model we introduced in [Section 3](#) directly becomes $P(N_{\text{sat}}|M, c)$, and

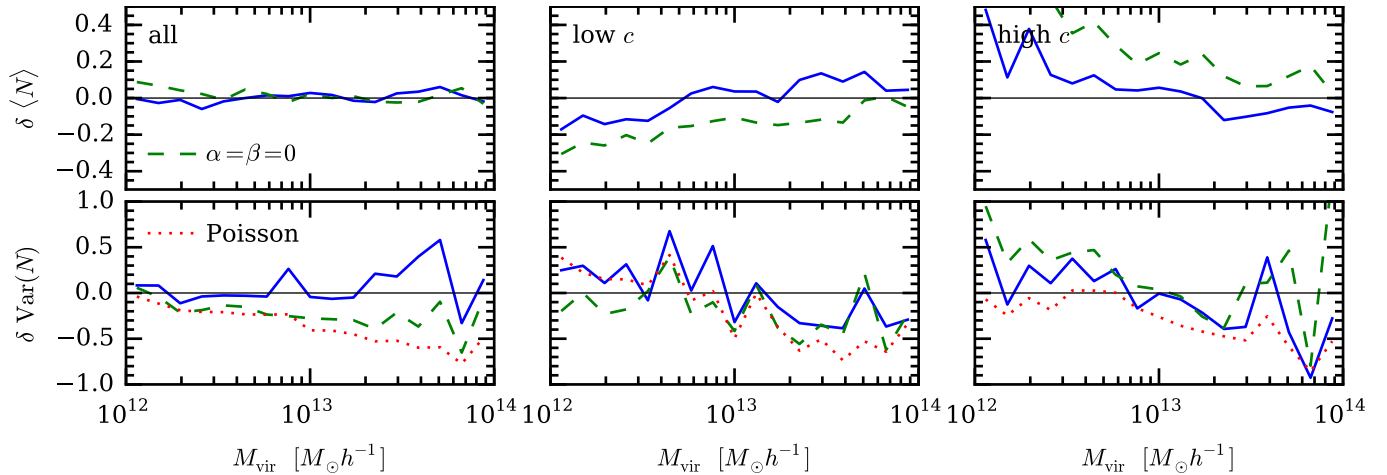


Figure 6. Relative difference between the model prediction and simulation of mean (upper row) and of variance (lower row) of the number of subhalos, in bins of host halo mass. The middle and the right columns show the lowest and the highest 25% of concentration, respectively. Blue solid line shows the model we present here. The green dashed line is a model that depends only on host halo mass (i.e., $\alpha = \beta = 0$). The red dotted line shows the Poisson scatter given the mean value in each bin.

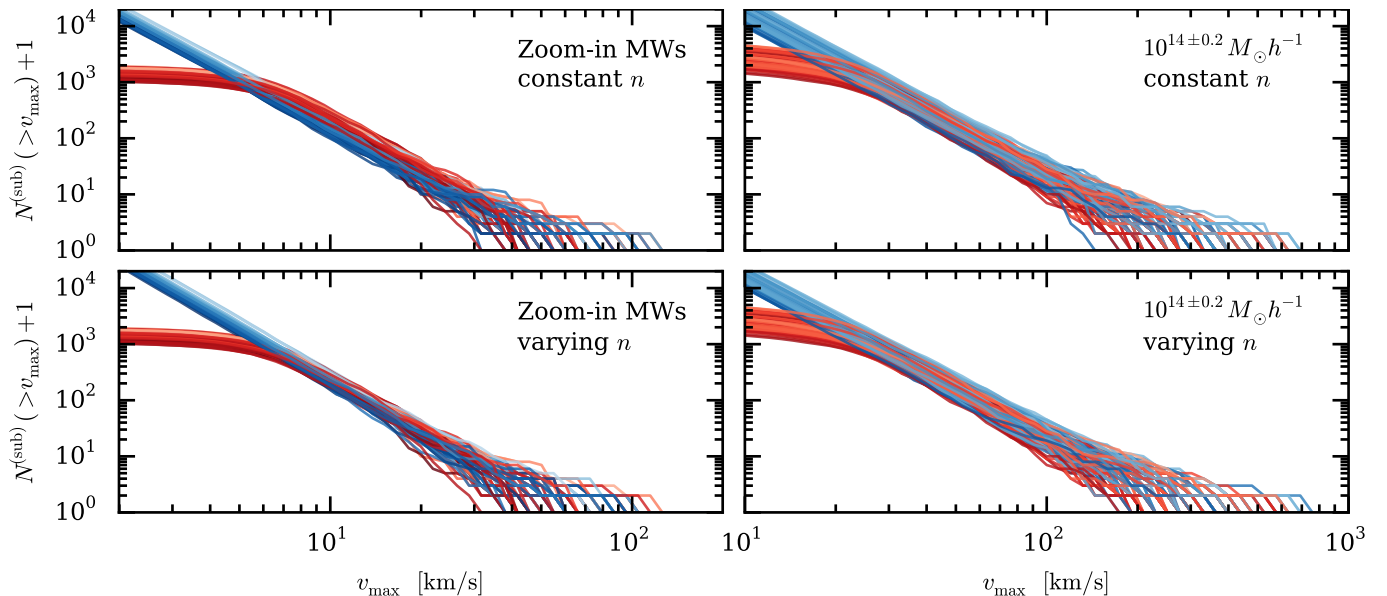


Figure 7. Subhalo abundance function in simulations (red) and predicted by the model (blue). The shade of colors represents the concentration ($V_{\text{max}}/V_{\text{vir}}$) of the halo: the darker the more concentrated. The two columns show two different host halo masses. The upper row uses the model with constant index ($n = n_0$), while the lower row uses Equation (9). The model with constant index cannot reproduce the subhalo abundance function for zoom-in Milky Way halos (upper left panel). The gray band on the left shows the regime affected by resolution.

it implies that satellite occupation depends on both host halo mass and concentration.

A different, but also widely used approach is to use Halo Occupation Distribution (HOD). Instead of specifying the galaxy–subhalo connection, standard HOD directly models the probability distribution of satellite occupation at a luminosity threshold as a function of host halo mass (e.g., Peacock & Smith 2000; Seljak 2000; Scocimarro et al. 2001; Berlind & Weinberg 2002; Cooray & Sheth 2002). That is, it specifies $P(N_{\text{sat}} > L|M)$, and this distribution of satellite occupation does not depend on host halo concentration. Nevertheless, one can also generalize the HOD to include the concentration dependence and to specify $P(N_{\text{sat}}|M, c)$. Yet most studies constraining HOD assume the sole dependence on mass.

Abundance matching and HOD also differ from each

other in how the positions of the satellite galaxies are assigned. However, in the context of satellite occupation, the only relevant difference is whether or not the satellite occupation depends on host halo concentration (at a given host halo mass). It is clear that *subhalo* occupation does depend on host halo concentration, but the stochastic process of galaxy formation could diminish this dependence. Nevertheless, it is also possible that Equation (10) is only perturbed, and the concentration dependence of *subhalo* abundance still survives and results in the concentration dependence of *satellite* abundance.

In this section, we assume the simple relation of Equation (10), and investigate the implications of the correlation between concentration and satellite occupation. We compare the different inferences between these two mod-

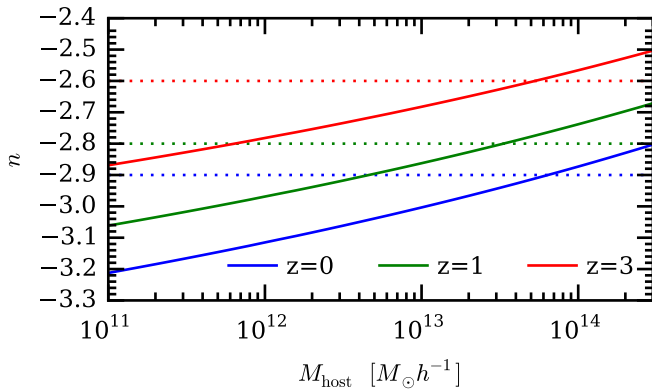


Figure 8. The solid lines show Equation (9): the log-log slope as a function of mass at three different redshifts: $z = 0$ (blue), 1 (green), and 3 (red). The dotted horizontal lines show the values of n_0 in Table 1 of corresponding redshifts.

els (with and without concentration dependence) when using satellite occupation as a proxy of halo mass. Then we look at the the possible signal of halo assembly bias with satellite occupation.

4.1. Satellite Occupation as a Proxy of Halo Mass

Satellite occupation, especially in the cluster-mass regime, has been used to probe the host halo mass (Old et al. 2014, 2015; Oguri & Lin 2015; Rozo et al. 2015). Conventionally, this is done within the standard HOD framework, which ignores the dependence of satellite occupation on host halo concentration. Here we would like to investigate the effects of ignoring this dependence. We consider the two subhalo models, as presented in Figure 6: one only depends on halo mass like the standard HOD, and the other incorporates the dependence on concentration as introduced in Section 3. We then take the host halos from simulations and populate them with subhalos according to these two models. This procedure is repeated multiple times to obtain enough statistics and to smooth the Poisson noise.

Figure 9 shows the joint distribution of the host halo mass and concentration at a fixed satellite occupation, $N_{\text{sat}}(v_{\text{max}} > 75 \text{ km/s}) = 100$, in the context of cluster-size halos. We see significant differences between the inferences from the two subhalo models, with or without the dependence on concentration. Although the mean value of inferred mass does not differ more than 1σ , the inferred distribution of mass is much wider in the case with the dependence on concentration, and also includes many more high-concentration high-mass or low-concentration low-mass halos.

The difference seen in Figure 9 would be especially prominent when the number of subhalos in consideration is large compared to the Poisson noise, i.e., $N_{\text{sat}} \gg \sqrt{N_{\text{sat}}}$. Thus when estimating the mass of galaxy clusters with richness or satellite occupation, one should consider including halo concentration in the model, especially in cases when not only the mean estimator but also the resulting inference is relevant.

To refine the mass estimator for halos of a fixed occupation, we then need some independent observable to probe halo concentration. We discuss three possible choices here.

1. *The radial distribution of satellites.* If satellites

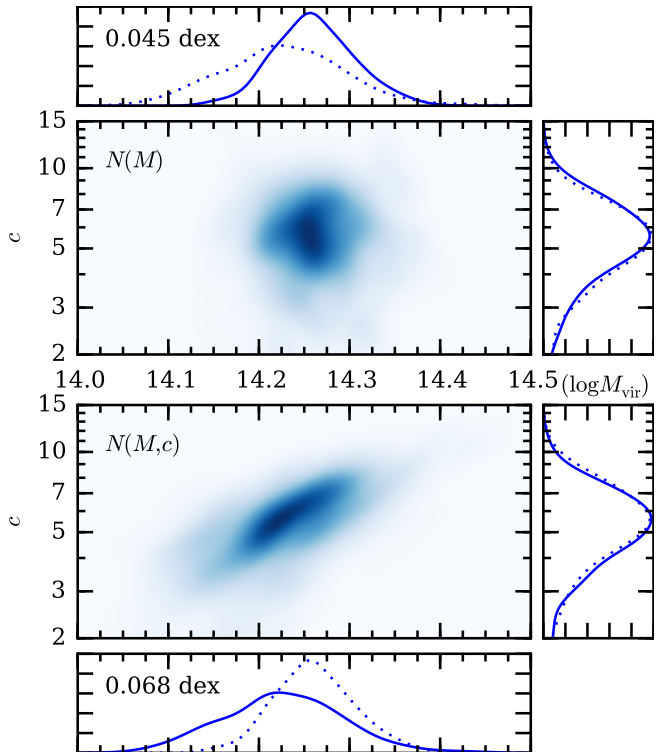


Figure 9. The joint and marginal distributions of logarithmic concentration (y -axis) and logarithmic mass (x -axis) of all the host halos which have exactly 100 subhalos whose $v_{\text{max}} > 75 \text{ km s}^{-1}$. The upper and lower parts demonstrate the inference from the two models: (1) with only mass dependence (upper) and (2) with both mass and concentration dependence (lower). Dotted lines in the side panels show the same marginal distribution for the other model just for convenient comparison by eyes. Both models are the same as used in Figure 6. The number in the marginal distribution of logarithmic mass shows σ value.

trace the density profile of the host halo, then by the radial distribution of satellites could provide independent information on host halo concentration. By comparing the number of satellites in different projected radial bins, one may be able to select those more concentrated halos in a fixed-richness sample.

2. *The luminosity of the central galaxy.* For example, the abundance matching scheme of Equation (10) matches luminosity with v_{max} or v_{peak} instead of M_{vir} , and results in the dependence of luminosity on concentration. Hence a further selection on the luminosity of central galaxy may provide a tighter mass distribution (see also Reyes et al. 2008). R. M. Reddick et al. (2015, in preparation) also finds a negative correlation between the central luminosity and richness at a fixed halo mass, which agrees with trends proposed here.
3. *The magnitude gap.* In addition to the concentration dependence of luminosity, the magnitude gap between the central galaxy and the brightest satellite galaxy can further depend on the host halo concentration. For instance, as suggested by our model, the parameter V_{cut} itself has a concentration dependence, regardless how luminosity is matched to halo properties. It has also been shown

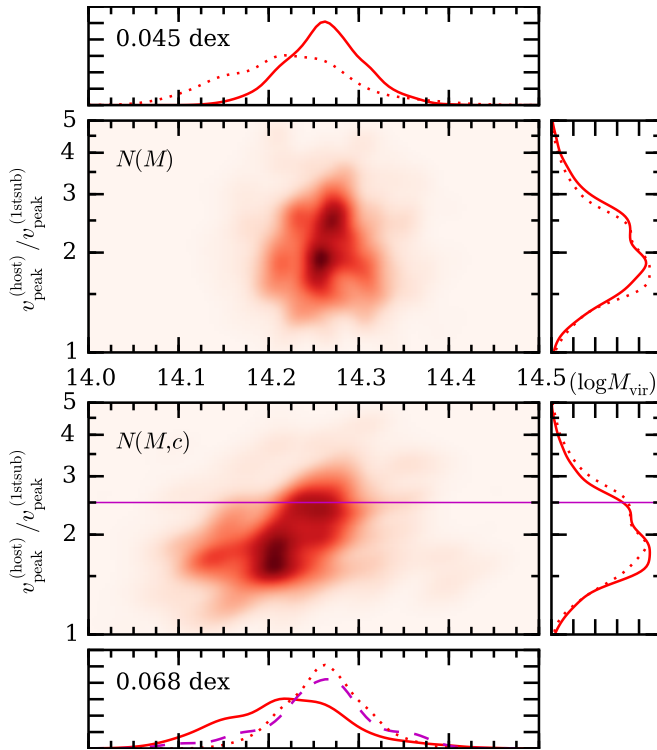


Figure 10. Same as Figure 9, but showing the distributions of $\log v_{\text{peak}}^{\text{host}}/v_{\text{peak}}^{\text{1stsub}}$ (y -axis) and logarithmic mass (x -axis). The magenta dashed line in the lowest panel shows the mass distribution when selecting only halos whose “gap” is larger than 2.5.

in simulations that the gap is correlated with the formation history of the host halo, and hence with concentration (D’Onghia et al. 2005; Zentner et al. 2005; Dariush et al. 2010; Deason et al. 2013; Wu et al. 2013).

It has been suggested that selecting on magnitude gap can refine the mass distribution of a fixed-richness sample (More 2012; Hearin et al. 2013; Lu et al. 2015). Here we revisit this method by considering the correlation between occupation (richness) and halo concentration. Figure 10 shows the distributions of magnitude gap and halo mass, for a sample of a fixed occupation (100 subhalos whose $v_{\text{max}} > 75 \text{ km s}^{-1}$, same as in Figure 9), for the two subhalo models. Here the magnitude gap is approximated by $\log v_{\text{peak}}^{\text{host}}/v_{\text{peak}}^{\text{1stsub}}$, and can be translated into the actual magnitude map by abundance matching. As we already learned, the distribution of halo mass is much wider (lower panel) than that from the assumption that satellite occupation depends on host halo mass only (upper panel). Nevertheless, if we apply a further selection on the magnitude gap, selecting only halos with larger gaps, we can obtain a sample of halos whose mass distribution is much closer to that in the upper panel.

This may provide a viable method to obtain a sample of halos in a narrower halo mass bin, especially in the high-mass regime. It has been shown that selecting on magnitude gap can indeed narrow the velocity dispersion distribution of the sample (Hearin et al. 2013). As for halo mass, it remains to be seen how strong these effects are in specific observed samples, but we expect that the relative impact of the central galaxy luminosity and the magnitude gap could be tested in the near future using

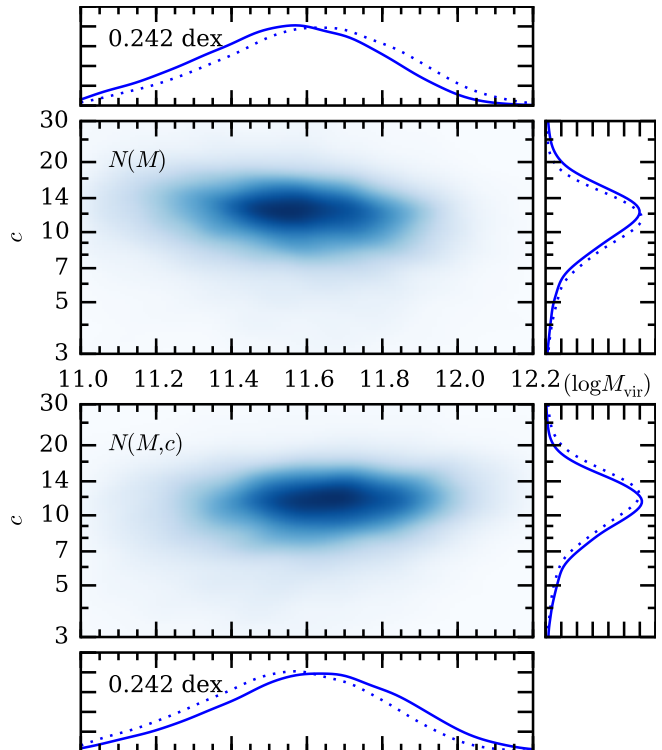


Figure 11. Same as Figure 9, but showing of all the host halos which have exactly four subhalos whose $v_{\text{max}} > 30 \text{ km s}^{-1}$.

either lensing or X-ray measurements of large samples of optically selected clusters with fixed galaxy number.

4.2. Satellites of Milky Way

In the context of Milky Way-mass halos, the number of subhalos in consideration is much smaller, and the Poisson noise of individual halos would dominate and diminish the difference between these two subhalo models. Nevertheless, in Figure 9 we observe a positive correlation between the host halo mass and concentration for this sample of a fixed satellite occupation. This positive correlation differs from the commonly known concentration–mass relation (e.g., Navarro et al. 1997), and can also be seen when the number of subhalos in consideration is small.

Figure 11 shows the joint distribution of the host halo mass and concentration at another fixed satellite occupation, $N_{\text{sat}}(v_{\text{max}} > 30 \text{ km/s}) = 4$. In this case, the marginal distributions of mass or of concentration barely differ between the two subhalo models. Nevertheless, the predicted correlation between mass and concentration is fairly different in the two cases. Without the dependence on concentration, a sample of a fixed satellite occupation basically corresponds to a sample of halos in a mass bin, and the correlation between halo concentration and mass inherits the usual, negative, concentration–mass relation of host halos. On the other hand, with the dependence on concentration, the inferred correlation between concentration and mass becomes positive.

This discrepancy again highlights the need to consider this dependence of satellite occupation on concentration when inferring the mass or other properties of the Milky Way halo from satellites (e.g., Busha et al. 2011a; Rodríguez-Puebla et al. 2013b,a; Cautun et al. 2014a).

If the inference is not derived completely from simulations but with the help of a subhalo model which does not account for dependence on concentration, such as the conventional HOD, then one might need to consider the effect discussed above when interpreting the results, particularly the degenerate correlation between concentration and mass. We also note that recent constraint on the mass and concentration of the Milky Way from dynamical tracers have a negatively correlated degeneracy (Wang et al. 2015), while occupation-based constraints will have the opposite degeneracy if the concentration dependence is properly accounted for, as demonstrated here.

This dependence on concentration also suggests that one should take the concentration of the Milky Way halo into account when investigating the tension between the population of subhalos in N -body simulations and that of the observed Milky Way satellite galaxies (e.g., Kauffmann et al. 1993; Klypin et al. 1999; Moore et al. 1999; Bullock 2010; Boylan-Kolchin et al. 2011; Purcell & Zentner 2012). While a Milky Way-like halo is conventionally defined by selecting on halo mass only, it is clear that the concentration of the Milky Way halo could potentially change the statistical significance of the aforementioned tension. In a follow-up paper, we further investigate these implications of this dependence on concentration for the Milky Way and its population of satellites (Y.-Y. Mao et al. 2015, in preparation).

4.3. Observing Halo Assembly Bias

Given that satellite occupation is a direct observable that is correlated with halo concentration, it may provide a way to observationally detect the halo assembly bias. Halo assembly bias has been shown to exist in simulations; particularly it is found that host halos of different formation histories or concentrations cluster differently,

$$b_h(M, c) \neq b_h(M), \quad (11)$$

where b_h is the halo bias function (Gao et al. 2005; Wechsler et al. 2006; Gao & White 2007). The question we want to address here is whether we can measure

$$b_h(M, N_{\text{sat}}) \neq b_h(M), \quad (12)$$

and if so, whether it implies the existence of halo assembly bias as in Equation (11).

Instead of calculating the bias function directly, we use the mark correlation function (MCF) to probe the bias. The MCF is defined as

$$\text{MCF}(m, r) = \sum_{(i,j) \in S_r} \frac{m_i m_j}{\bar{m}^2}, \quad (13)$$

where $S_r = \{(i, j) : |\mathbf{x}_i - \mathbf{x}_j| \in [r, r + dr]\}$, and \bar{m} is the mean of m_i over i . The MCF of a specific mark m shows whether the averaged value of this mark for halos in pairs is higher or lower than the averaged value of the whole sample. For each radial bin S_r , we find all pairs of halos whose separation falls in that bin and measure the mark of those halos. To accommodate the possible large range of the mark values, we use the ranks of the mark instead of the actual value for m , normalized by the total number of different values. If Equation (12) holds, we expect either a positive or a negative excess in the MCF of N_{sat} .

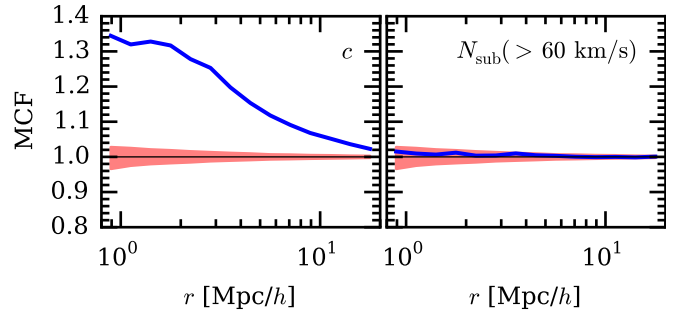


Figure 12. The MCFs of concentration (left) and of satellite occupation ($v_{\text{max}} > 60 \text{ km s}^{-1}$) (right), for host halos whose mass is within 10^{11} and $10^{11.4} M_{\odot} h^{-1}$. The red shaded area shows the range of MCF consistent with no correlation within $2\text{-}\sigma$.

In Wechsler et al. (2006), the authors found a positive excess in the MCF of N_{sat} in the regime above M_* , but were not able to find a similar signal below M_* . To interpret these results, recall that for halos below the typical collapse mass M_* , high-concentrated halos are more clustered; for halos above M_* , high-concentrated halos are less clustered. In the regime above M_* , halos in pairs are on averaged more massive but *less* concentrated, and both characters give a higher N_{sat} . As a result, the excess in the MCF of N_{sat} comes from a mixed effect of both mass and concentration, and hence it is easy to detect this excess but would be difficult to distinguish whether this signal is really coming from halo assembly bias.

On the other hand, in the regime below M_* , the dependence of the clustering strength on halo concentration switches sign, but the dependence of N_{sat} on concentration remains the same: host halos that form earlier still have fewer subhalos at a fixed mass. As a result, in the regime below M_* , halos in pairs are on averaged more massive and *more* concentrated, and these two characters have opposite effects on N_{sat} . If a negative excess in the MCF of N_{sat} is detected, this signal must come from the contribution of concentration, or halo assembly bias. However, in Wechsler et al. (2006), there were not enough subhalos resolved in the simulation for the correlation between subhalo abundance and halo concentration to manifest itself, and hence this signal was not detected.

We first calculate the MCFs of halo concentration and of satellite occupation by selecting all resolved subhalos whose $v_{\text{max}} > 60 \text{ km s}^{-1}$ in our cosmological box, for host halos in a mass range, $10^{11}\text{--}10^{11.4} M_{\odot} h^{-1}$, and plot the results in Figure 12. The result we found here is consistent with previous studies: significant bias in concentration, but not in satellite occupation. This result, however, does not directly answer whether or not the satellite occupation can probe assembly bias, because the variance in N_{sat} can be large. As we argued in Section 3,

$$(N_{\text{sat}}|M, c) \sim \text{Pois}(\langle N_{\text{sat}}|M, c \rangle). \quad (14)$$

For host halos in this mass range, the number of resolved subhalos is typically less than 10, even for a high-resolution cosmological box (e.g., with a particle mass of $10^7 M_{\odot} h^{-1}$). Despite the correlation between subhalo abundance and host halo concentration, the scatter in subhalo abundance can wash out this correlation, especially for host halos with few subhalos, and render the bias in subhalo occupation unobservable.

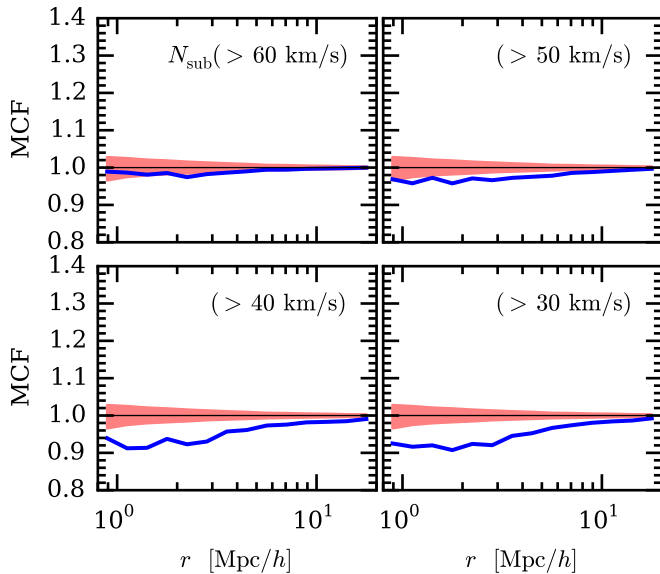


Figure 13. Same as Figure 12, but shows the MCFs of *model-predicted* satellite occupation down to 60, 50, 40, and 30 km s^{-1} . The corresponding number densities are 0.122, 0.216, 0.38, 1.03 $(\text{Mpc}/h)^{-3}$.

To verify our conjecture that Equation (12) would hold for low-mass halos if the typical value of N_{sat} is large (> 10), one would need a cosmological box large enough to measure clustering statistics and with a particle mass of $\sim 10^5 M_{\odot} h^{-1}$, but this kind of simulation is still beyond the reach of current computational capabilities. Zoom-in simulations can easily provide a much better resolution, but those do not provide large-scale statistics. With our model, we can predict the expected number of subhalos (satellites) to a lower velocity cut (higher number density), while preserving the dependence on host halo mass and concentration. We then can quantify at what velocity cut (number density) we can start to observe the bias in subhalo occupation in low-mass host halos.

Figure 13 shows the model-predicted MCF of subhalo occupation for four different thresholds, in the same mass range of the host halos, $10^{11} - 10^{11.4} M_{\odot} h^{-1}$. The host halos are selected from the cosmological box, and for each host halo we re-populate its subhalos with our model. At $v_{\text{max}} = 60 \text{ km s}^{-1}$ the result can be directly compared with the right panel of Figure 12. Since our model by construction correlates subhalo abundance and halo concentration ($V_{\text{max}}/V_{\text{vir}}$), the lack of signal in the MCF at $v_{\text{max}} = 60 \text{ km s}^{-1}$ results from the Poisson scatter. Moving the threshold down to $v_{\text{max}} = 40 \text{ km s}^{-1}$ we start to see a clear negative excess in the MCF. As we discussed above, this negative excess must originate from the fact that paired halos are on averaged more concentrated, and hence have fewer subhalos.

This negative excess in the MCF would manifest in the projected correlation function by lowering the one-halo term if the low-threshold data is available. With upcoming deep spectroscopic surveys, such as DESI (Levi et al. 2013), data with low thresholds will be accessible in the near future. Figure 14 demonstrates the number of galaxies in a volume-limited sample from two exemplary surveys, assuming the luminosity function reported in Blanton et al. (2003, 2005). Both surveys have

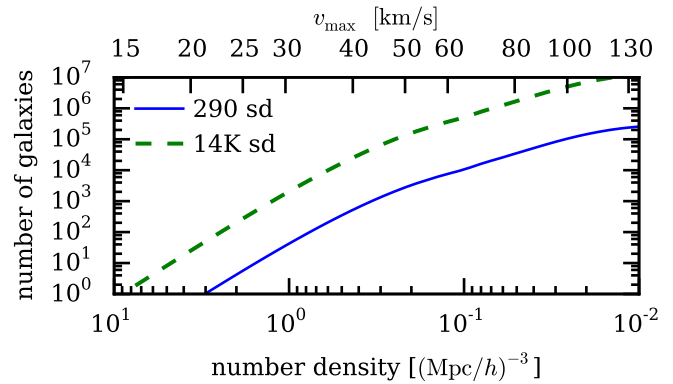


Figure 14. Expected number of galaxies in a volume-limited sample as a function of number density (and corresponding halo v_{max}) for two example surveys with different sky coverage (given in square degrees).

a detection limit of $m_r = 19.5$, and their sky coverages are 290 and 14,000 square degrees, roughly representing the GAMA Survey⁹ (Driver et al. 2011) and the DESI Bright Galaxy Survey,¹⁰ respectively. With the latter survey, a volume-limited sample of a few hundred thousand galaxies with $m_r < 19.5$ down to the number density at $0.4 (\text{Mpc}/h)^{-3}$ would be accessible, and this sample would be sufficient for a precise measurement of the projected correlation function.

We note that although we assume the simple relation of Equation (10) in this discussion, this signal has the advantage that it is less sensitive to the details of the galaxy-halo relation because it only utilizes the number of satellites above a certain luminosity threshold, but not other properties (e.g., color) of the satellites. Even if galaxy formation introduces additional scatter in the satellite occupation, as long as this scatter is smaller than the halo-to-halo scatter due to halo concentration, this signal would survive in the projected correlation function.

5. SUMMARY

In this work, we model the subhalo abundance on the basis of individual halos. The framework of our model is based on the fact that the scatter in N_{sub} for an *individual* halo is consistent with Poisson scatter, and the additional halo-to-halo scatter in N_{sub} for halos *in a mass bin* primarily affects only the overall normalization of the subhalo function. For a large sample of halos, we find that the subhalo velocity functions of a sample of halos in a mass range are nearly parallel to one another. As a result, we can model this halo-to-halo scatter by introducing additional parameters to the model that specify the normalization as a function of additional halo properties.

We hence present a model which predicts the subhalo abundance based on two properties: V_{vir} (equivalent to mass) and $V_{\text{max}}/V_{\text{vir}}$ (roughly equivalent to concentration) of the host halos. This model successfully reproduces the mean and scatter in the subhalo abundance in a given host halo mass bin. It can then be used to predict the number of subhalos for thresholds that are lower than the resolution limit of the simulation. It also

⁹ <http://www.gama-survey.org/>

¹⁰ <http://desi.lbl.gov/cdr/>

enables one to conveniently sample a sequence of v_{\max} values that represent the subhalos of a given host halo.

This model further provides plain insight into the dependence of subhalo abundance on halo concentration. We found that the halo concentration affects the subhalo abundance function mainly through the overall normalization (V_0 in our parameterization), but also through the “cutoff” scale (V_{cut}). A constant power-law index (n) fits the cosmological simulations well; however, we also find that an index that depends on halo mass would fit the zoom-in Milky Way halos better. This dependence on mass may have the same physical origin as the dependence on redshift.

With this model, we then investigate the observable implications of the correlation between the subhalo abundance and halo concentration. We find that when using subhalo or satellite occupation as a proxy of halo mass, one might need to consider using a concentration-dependent model, such as the one presented here, to obtain a more accurate inference. We show that ignoring this dependence on concentration could result in a biased mass inference and an incorrect joint distribution of mass and concentration of the sample. Although these biases are small, they may become important as other sources of systematic errors decrease.

We further propose that satellite occupation can be used to probe halo assembly bias if we can detect all satellites which reside in subhalos down to $\sim 40 \text{ km s}^{-1}$. Because in the low-mass regime, high-concentration halos are more clustered but have fewer subhalos, this signal can probe the halo assembly bias in concentration and is *not* degenerate with the contribution from halo mass. This method is also less sensitive to the detailed galaxy formation processes because it only depends on the total count.

Y. Y. M is supported by a Weiland Family Stanford Graduate Fellowship. M. W. received support from Stanford University grants for summer research. This work was supported in part by the U.S. Department of Energy contract to SLAC No. DE-AC02-76SF00515. We thank Matthew Becker for providing access to the cosmological simulations (c125-2048 and c125-1024) used in this work. We thank Tom Abel, Matthew Becker, Peter Behroozi, Michael Boylan-Kolchin, Andrew Hearin, Eduardo Rozo, and Andrew Zentner for helpful discussions and comments. Y. Y. M thanks CCAPP for its hospitality and for useful discussion with participants at a Fall 2014 workshop on assembly bias. The simulations used were run using computational resources at SLAC; we gratefully acknowledge the support of the SLAC computational team. This research also used resources of the National Energy Research Scientific Computing Center, a DOE Office of Science User Facility supported by the Office of Science of the U.S. Department of Energy under Contract No. DE-AC02-05CH11231.

REFERENCES

- Allgood, B., Flores, R. A., Primack, J. R., et al. 2006, *MNRAS*, 367, 1781
 Angulo, R. E., Lacey, C. G., Baugh, C. M., & Frenk, C. S. 2009, *MNRAS*, 399, 983
 Behroozi, P. S., Wechsler, R. H., & Wu, H.-Y. 2013a, *ApJ*, 762, 109
 Behroozi, P. S., Wechsler, R. H., Wu, H.-Y., et al. 2013b, *ApJ*, 763, 18
 Berlind, A. A., & Weinberg, D. H. 2002, *ApJ*, 575, 587
 Blanton, M. R., Lupton, R. H., Schlegel, D. J., et al. 2005, *ApJ*, 631, 208
 Blanton, M. R., Hogg, D. W., Bahcall, N. A., et al. 2003, *ApJ*, 592, 819
 Boylan-Kolchin, M., Bullock, J. S., & Kaplinghat, M. 2011, *MNRAS*, 415, L40
 Boylan-Kolchin, M., Springel, V., White, S. D. M., & Jenkins, A. 2010, *MNRAS*, 406, 896
 Bullock, J. S. 2010, *ArXiv e-prints*, arXiv:1009.4505
 Bullock, J. S., Kolatt, T. S., Sigad, Y., et al. 2001, *MNRAS*, 321, 559
 Busha, M. T., Marshall, P. J., Wechsler, R. H., Klypin, A., & Primack, J. 2011a, *ApJ*, 743, 40
 Busha, M. T., Wechsler, R. H., Behroozi, P. S., et al. 2011b, *ApJ*, 743, 117
 Cautun, M., Frenk, C. S., van de Weygaert, R., Hellwing, W. A., & Jones, B. J. T. 2014a, *MNRAS*, 445, 2049
 Cautun, M., Hellwing, W. A., van de Weygaert, R., et al. 2014b, *MNRAS*, 445, 1820
 Conroy, C., Wechsler, R. H., & Kravtsov, A. V. 2006, *ApJ*, 647, 201
 Cooray, A., & Sheth, R. 2002, *Phys. Rep.*, 372, 1
 Croce, M., Puelblas, S., & Scoccimarro, R. 2006, *MNRAS*, 373, 369
 Cui, W., Borgani, S., Dolag, K., Murante, G., & Tornatore, L. 2012, *MNRAS*, 423, 2279
 Dariush, A. A., Raychaudhury, S., Ponman, T. J., et al. 2010, *MNRAS*, 405, 1873
 Deason, A. J., Conroy, C., Wetzel, A. R., & Tinker, J. L. 2013, *ApJ*, 777, 154
 D’Onghia, E., Sommer-Larsen, J., Romeo, A. D., et al. 2005, *ApJL*, 630, L109
 Driver, S. P., Hill, D. T., Kelvin, L. S., et al. 2011, *MNRAS*, 413, 971
 Gao, L., Navarro, J. F., Frenk, C. S., et al. 2012, *MNRAS*, 425, 2169
 Gao, L., Springel, V., & White, S. D. M. 2005, *MNRAS*, 363, L66
 Gao, L., & White, S. D. M. 2007, *MNRAS*, 377, L5
 Gao, L., White, S. D. M., Jenkins, A., Stoehr, F., & Springel, V. 2004, *MNRAS*, 355, 819
 Garrison-Kimmel, S., Boylan-Kolchin, M., Bullock, J. S., & Lee, K. 2014, *MNRAS*, 438, 2578
 Giocoli, C., Pieri, L., & Tormen, G. 2008, *MNRAS*, 387, 689
 Hahn, O., & Abel, T. 2011, *MNRAS*, 415, 2101
 Hearin, A. P., Zentner, A. R., Newman, J. A., & Berlind, A. A. 2013, *MNRAS*, 430, 1238
 Ishiyama, T., Fukushige, T., & Makino, J. 2009, *ApJ*, 696, 2115
 Ishiyama, T., Rieder, S., Makino, J., et al. 2013, *ApJ*, 767, 146
 Jiang, F., & van den Bosch, F. C. 2014, *ArXiv e-prints*, arXiv:1403.6827
 Kauffmann, G., White, S. D. M., & Guiderdoni, B. 1993, *MNRAS*, 264, 201
 Klypin, A., Kravtsov, A. V., Valenzuela, O., & Prada, F. 1999, *ApJ*, 522, 82
 Kravtsov, A. V., Berlind, A. A., Wechsler, R. H., et al. 2004, *ApJ*, 609, 35
 Levi, M., Bebek, C., Beers, T., et al. 2013, *ArXiv e-prints*, arXiv:1308.0847
 Lu, Y., Yang, X., & Shen, S. 2015, *ApJ*, 804, 55
 Macciò, A. V., Dutton, A. A., van den Bosch, F. C., et al. 2007, *MNRAS*, 378, 55
 Moore, B., Ghigna, S., Governato, F., et al. 1999, *ApJL*, 524, L19
 More, S. 2012, *ApJ*, 761, 127
 Navarro, J. F., Frenk, C. S., & White, S. D. M. 1997, *ApJ*, 490, 493
 Oguri, M., & Lin, Y.-T. 2015, *ApJ*, 801, 94
 Old, L., Skibba, R. A., Pearce, F. R., et al. 2014, *MNRAS*, 441, 1513
 Old, L., Wojtak, R., Mamon, G. A., et al. 2015, *MNRAS*, 449, 1897
 Peacock, J. A., & Smith, R. E. 2000, *MNRAS*, 318, 1144
 Purcell, C. W., & Zentner, A. R. 2012, *J. Cosmology Astropart. Phys.*, 12, 7
 Reddick, R. M., Wechsler, R. H., Tinker, J. L., & Behroozi, P. S. 2013, *ApJ*, 771, 30
 Reyes, R., Mandelbaum, R., Hirata, C., Bahcall, N., & Seljak, U. 2008, *MNRAS*, 390, 1157
 Rodríguez-Puebla, A., Avila-Reese, V., & Drory, N. 2013a, *ApJ*, 767, 92
 —. 2013b, *ApJ*, 773, 172
 Rozo, E., Rykoff, E. S., Bartlett, J. G., & Melin, J.-B. 2015, *MNRAS*, 450, 592
 Rozo, E., Rykoff, E. S., Koester, B. P., et al. 2009, *ApJ*, 703, 601
 Rozo, E., Wechsler, R. H., Rykoff, E. S., et al. 2010, *ApJ*, 708, 645

- Scoccimarro, R., Sheth, R. K., Hui, L., & Jain, B. 2001, *ApJ*, 546, 20
- Seljak, U. 2000, *MNRAS*, 318, 203
- Springel, V. 2005, *MNRAS*, 364, 1105
- Springel, V., Yoshida, N., & White, S. D. M. 2001, *New A*, 6, 79
- Springel, V., Wang, J., Vogelsberger, M., et al. 2008, *MNRAS*, 391, 1685
- Vale, A., & Ostriker, J. P. 2004, *MNRAS*, 353, 189
- van den Bosch, F. C., & Jiang, F. 2014, *ArXiv e-prints*, arXiv:1403.6835
- Vogelsberger, M., Genel, S., Springel, V., et al. 2014, *MNRAS*, 444, 1518
- Wang, W., Han, J., Cooper, A., et al. 2015, *ArXiv e-prints*, arXiv:1502.03477
- Watson, D. F., Berlind, A. A., & Zentner, A. R. 2011, *ApJ*, 738, 22
- Wechsler, R. H., Bullock, J. S., Primack, J. R., Kravtsov, A. V., & Dekel, A. 2002, *ApJ*, 568, 52
- Wechsler, R. H., Zentner, A. R., Bullock, J. S., Kravtsov, A. V., & Allgood, B. 2006, *ApJ*, 652, 71
- Wu, H.-Y., Hahn, O., Wechsler, R. H., Behroozi, P. S., & Mao, Y.-Y. 2013, *ApJ*, 767, 23
- Yang, X., Mo, H. J., Zhang, Y., & van den Bosch, F. C. 2011, *ApJ*, 741, 13
- Zehavi, I., Zheng, Z., Weinberg, D. H., et al. 2011, *ApJ*, 736, 59
- Zentner, A. R., Berlind, A. A., Bullock, J. S., Kravtsov, A. V., & Wechsler, R. H. 2005, *ApJ*, 624, 505
- Zhu, G., Zheng, Z., Lin, W. P., et al. 2006, *ApJL*, 639, L5